Dipole response of ^{88}Sr up to the neutron-separation energy

R. Schwengner,[1] G. Rusev,[1] N. Benouaret,[1,2] R. Beyer,[1] M. Erhard,[1] E. Grosse,[1,3] A. R. Junghans,[1] J. Klug,[1] K. Kosev,[1] L. Kostov,[4] C. Nair,[1] N. Nankov,[1,4] K. D. Schilling,[1] and A. Wagner[1]

[1]*Institut für Strahlenphysik, Forschungszentrum Dresden-Rossendorf, Postfach 510119, D-01314 Dresden, Germany*

[2]*Faculté de physique, Université des Sciences et de la technologie d'Alger, El-Alia 16111, Bab-Ezzouar-Alger, Algerie*

[3]*Institut für Kern- und Teilchenphysik, Technische Universität Dresden, D-01062 Dresden, Germany*

[4]*Institute for Nuclear Research and Nuclear Energy, BAS, BG-1784 Sofia, Bulgaria*

(Received 14 February 2007; published 24 September 2007)

The dipole response of the magic $N = 50$ nucleus ^{88}Sr was studied in photon-scattering experiments at the electron linear accelerator ELBE with bremsstrahlung produced at kinetic electron energies of 9.0, 13.2, and 16.0 MeV. We identified 160 levels up to an excitation energy of 12 MeV. By using polarized photons linear polarizations of about 50 γ transitions were measured that enabled parity assignments to the corresponding states. In the energy range of 6–12 MeV we identified only one $M1$ transition; all other transitions have $E1$ character. Thus, $E1$ character was proven for 63% of the total dipole strength of the observed levels in the given energy range. Statistical methods were applied to estimate intensities of inelastic transitions and to correct the intensities of the ground-state transitions for their branching ratios. In this way we derived the photoabsorption cross section up to the neutron-separation energy. This cross section matches well the photoabsorption cross section obtained from (γ, n) data and thus provides information about the extension of the dipole-strength distribution toward energies below the neutron-separation energy. An enhancement of $E1$ strength at 6–11 MeV may be considered as an indication for a pygmy dipole resonance.

DOI: 10.1103/PhysRevC.76.034321 PACS number(s): 25.20.Dc, 21.10.Tg, 21.60.Cs, 27.50.+e

I. INTRODUCTION

The detailed understanding of the response of atomic nuclei to photons has received increasing attention in recent years. Information on the dipole strength at the low-energy tail of the giant dipole resonance (GDR) is important for an estimate of the effect of high temperatures during the formation of heavy elements in the cosmos. In particular, reaction rates in the so-called p-process are influenced by the behavior of dipole-strength distributions close to the neutron-separation energy [1]. This behavior may be affected by excitations such as the pygmy dipole resonance (see, e.g., Refs. [2–4]).

So far, estimates of the dipole strength obtained from calculations within a quasiparticle-random-phase approximation for spherical nuclei with a phenomenological implementation of nuclear deformation have been used for astrophysical applications [5,6]. A systematic investigation of the dipole strength with varying nucleon numbers and, thus, varying properties such as deformation is mandatory for the improvement of models that are used for modeling processes for the production of heavy elements in the cosmos.

Dipole-strength distributions up to the neutron-separation energies have been studied for only a few nuclides in experiments with monoenergetic photons (see, e.g., Refs. [7–10]) and in experiments with bremsstrahlung (see, e.g., Ref. [11] and references therein). The new bremsstrahlung facility [12] at the superconducting electron accelerator ELBE of the Research Center Dresden-Rossendorf opens up the possibility of studying the dipole response of stable nuclei with even the highest neutron-separation energies in photon-scattering experiments.

In the course of a systematic study of dipole-strength distributions for varying neutron and proton numbers in nuclei around $A = 90$ we started with the magic $N = 50$ nuclide ^{88}Sr. The lowest 2^+ state at 1836 keV, the lowest 1^+ state at 3486 keV, and seven further $J = 1$ states with intense ground-state transitions at 4743, 6212, 6333, 7089, 7534, 7838, and 8041 keV had been investigated in previous work [13–16]. In an experiment with monoenergetic photons the elastic scattering to the ground state and the inelastic scattering to the first excited state in ^{88}Sr were studied [8]. For the $J = 1$ states at 6212, 6333, 7089, 7838, and 8041 keV, negative parities were derived from an experiment with polarized photons [17]. For the state at 4743 keV, negative parity was determined in a measurement with a highly polarized, quasimonoenergetic photon beam [18]. Recently, a photon-scattering experiment at an electron energy of 6.8 MeV [19] was performed, in which 22 states were identified.

In the present study we observed about 160 transitions in the energy range from 7 to 12 MeV for the first time; 24 of these were just above the neutron-separation energy. We applied statistical methods to account for strength in the continuum part of the spectrum and to correct the dipole strength distribution for inelastic transitions depopulating high-lying levels to low-lying levels.

II. EXPERIMENTAL METHODS AND RESULTS

The nuclide ^{88}Sr was studied in photon-scattering experiments at the superconducting electron accelerator ELBE of the Research Center Dresden-Rossendorf. Bremsstrahlung was produced with electron beams of 9.0, 13.2, and 16.0 MeV kinetic energy and with average currents of 520, 400, and 420 μA hitting radiators consisting of niobium foils of 4, 7, and 2 μm thickness, respectively. A 10 cm thick

aluminum absorber was placed behind the radiator in to reduce the low-energy part of the bremsstrahlung spectrum. The collimated photon beam impinged onto the target with a flux of several 10^8 MeV^{-1} s^{-1} in a spot with 38 mm diameter. The target had a diameter of about 20 mm to enable an irradiation with a constant flux density over the target area. The target consisted of 2731.8 mg of $^{88}SrCO_3$ enriched to 99.9%, combined with 455.5 mg of ^{11}B used for the determination of the photon flux. Scattered photons were measured with four high-purity germanium (HPGe) detectors of 100% efficiency relative to a 3 × 3 in. NaI detector. All HPGe detectors were surrounded by escape-suppression shields made of bismuth germanate scintillation detectors. Two HPGe detectors were placed vertically at 90° relative to the photon-beam direction at a distance of 28 cm from the target. The other two HPGe detectors were positioned in a horizontal plane and can be moved between 90° to the beam at a distance of 28 cm from the target and 127° to the beam at a distance of 32 cm from the target. The position at 90° allows us to measure azimuthal asymmetries of the γ-ray intensities in an experiment with polarized photons and the position at 127° allows us to deduce angular distributions of the γ rays. Absorbers of 8 mm Pb plus 3 mm Cu were placed in front of the detectors at 127° whereas for the detectors at 90° absorbers of 13 mm Pb plus 3 mm Cu and of 15 mm Pb plus 3 mm Cu were used in the experiments at 9.0 and 13.2 MeV electron energy, respectively. A detailed description of the bremsstrahlung facility is given in Ref. [12].

Spectra of scattered photons were measured for 80 and 84 h in the experiments at 9.0 and 13.2 MeV electron energy, respectively. Parts of a spectrum including events measured with the two detectors placed at 127° relative to the beam at an electron energy of 13.2 MeV are shown in Fig. 1. At about 11.5 MeV the intensity drops remarkably. The neutron-separation energy of ^{88}Sr is $S_n = 11.1$ MeV. However, the ground-state spin of the isotope ^{87}Sr produced in the ^{88}Sr(γ, n) reaction is $9/2^+$. A population of this state following the emission of a low-energy neutron from the ground state of ^{88}Sr is hindered by the angular momentum barrier with $l = 4$. Alternatives may be the neutron emission from an excited 1^- state ($l = 3$) or the population of the $1/2^-$ isomer at 389 keV in ^{87}Sr, which leads to an effective opening of the neutron-emission channel around 11.5 MeV. The latter is proven by calculations using the code TALYS [20], which predict that the cross section for the population of the ground state of ^{87}Sr increases to about 1 mb at 11.4 MeV and stays constant at higher energies while the population of the isomer starts at 11.5 MeV with a cross section of about 10 mb and increases in agreement with the measured (γ, n) cross sections [21,22].

A. The photon-scattering method

In photon-scattering experiments the integrated scattering cross section I_s of an excited state at the energy E_x can be deduced from the measured rate of the respective transition to the ground state (elastic scattering). It can be determined relative to the known integrated scattering cross section of

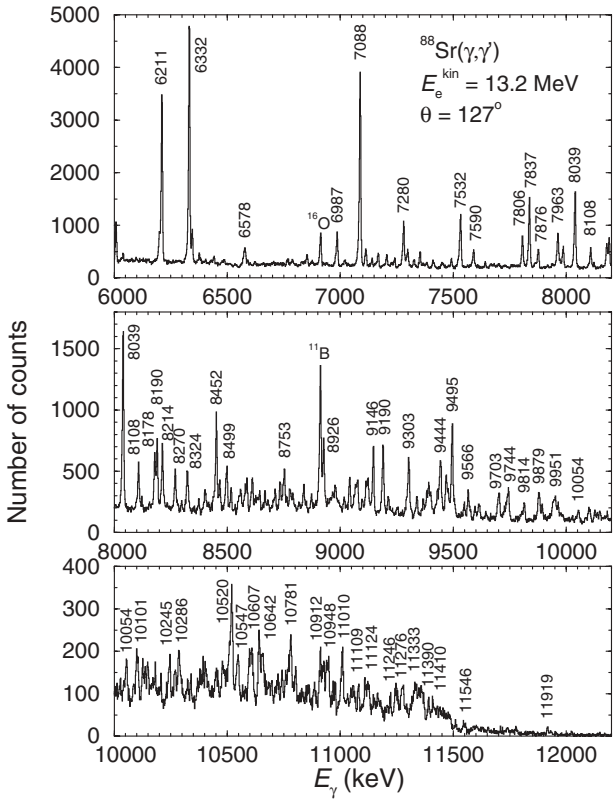

FIG. 1. Parts of a spectrum of photons scattered from ^{88}Sr combined with ^{11}B during the irradiation with bremsstrahlung produced by electrons of an energy of $E_e^{\rm kin} = 13.2$ MeV. This spectrum is the sum of the spectra measured with the two detectors placed at 127° relative to the beam. The most dominant transitions assigned to ^{88}Sr are marked with their energies in keV. The drop of intensity around 11.5 MeV is related to the opening of the (γ, n) channel.

states in ^{11}B [23]:

$$\frac{I_s(E_x)}{I_s\left(E_x^{\rm B}\right)} = \left(\frac{\dot{N}_\gamma(E_\gamma,\theta)}{W(E_\gamma,\theta)\Phi_\gamma(E_x)N_N}\right) \times \left(\frac{\dot{N}_\gamma\left(E_\gamma^{\rm B},\theta\right)}{W\left(E_\gamma^{\rm B},\theta\right)\Phi_\gamma\left(E_x^{\rm B}\right)N_N^{\rm B}}\right)^{-1}. \quad (1)$$

Here, $\dot{N}_\gamma(E_\gamma,\theta)$ and $\dot{N}_\gamma(E_\gamma^{\rm B},\theta)$ denote the measured rates of a considered ground-state transition at E_γ and of a ground-state transition in ^{11}B at $E_\gamma^{\rm B}$, respectively, observed at an angle θ to the beam, and $W(E_\gamma,\theta)$ and $W(E_\gamma^{\rm B},\theta)$ describe the angular correlations of these transitions. The quantities N_N and $N_N^{\rm B}$ are the numbers of nuclei in the ^{88}Sr and ^{11}B targets, respectively. The quantities $\Phi_\gamma(E_x)$ and $\Phi_\gamma(E_x^{\rm B})$ stand for the photon fluxes at the energy of the considered level and at the energy of a level in ^{11}B, respectively.

The integrated scattering cross section is related to the level width according to

$$I_s = \int \sigma_{\gamma\gamma} dE = \left(\frac{\pi\hbar c}{E_x}\right)^2 \frac{2J_x+1}{2J_0+1}\frac{\Gamma_0^2}{\Gamma}, \quad (2)$$

where $\sigma_{\gamma\gamma}$ is the elastic scattering cross section, and E_x, J_x, and Γ denote the energy, the spin, and the total width of the

excited level, respectively. The quantities J_0 and Γ_0 are the spin of the ground state and the partial width for the ground-state transition, respectively.

For the determination of the level widths one is faced with two problems. First, a considered level can be fed by transitions from higher lying states. The measured intensity of the ground-state transition is in this case higher than the one resulting from a direct excitation only. As a consequence, the integrated cross section deduced from this intensity contains a part originating from feeding in addition to the true integrated scattering cross section: $I_{s+f} = I_s + I_f$. Furthermore, a considered level can de-excite not only to the ground state but also to other low-lying states (inelastic scattering). In this case, not all observed γ transitions are ground-state transitions. To deduce the partial width of a ground-state transition Γ_0 and the integrated absorption cross section one has to know the branching ratio $b_0 = \Gamma_0/\Gamma$. If this branching ratio cannot be determined, only the quantity Γ_0^2/Γ can be deduced [cf. Eq. (2)].

B. Detector response and photon flux

For the analysis of the spectra the relative efficiency of the detectors and the relative photon flux are needed. Especially for the determination of the dipole-strength distribution described in Sec. III the experimental spectrum has to be corrected for detector response, for the absolute efficiency and the absolute photon flux, for background radiation, and for atomic processes induced by the impinging photons in the target material. The detector response has been simulated by using the program package GEANT3 [24]. The reliability of the simulation was tested by comparing simulated spectra with measured ones. As an example, a spectrum measured during the irradiation of a ^{12}C target with bremsstrahlung produced by electrons of an energy of $E_e^{\mathrm{kin}} = 17$ MeV is compared with the corresponding simulated one in Fig. 2. The simulated spectrum

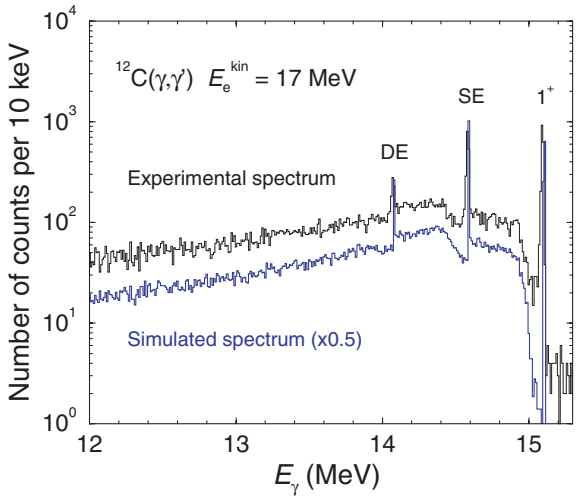

FIG. 2. (Color online) Spectrum of photons scattered from a ^{12}C sample at $E_e^{\mathrm{kin}} = 17$ MeV (black line) and spectrum simulated for the same conditions (blue line). The spectrum contains the ground-state transition from the 1^+ state at 15.110 MeV, its single-escape (SE) and double-escape (DE) peaks and the Compton background. The two spectra are very close to each other. To make them distinguishable, the simulated spectrum was multiplied by a factor of 0.5.

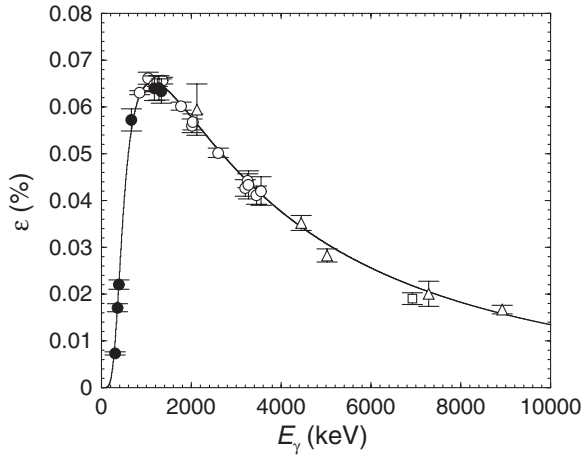

FIG. 3. Absolute efficiency of the two detectors at 127° measured by using ^{22}Na, ^{60}Co, ^{133}Ba, and ^{137}Cs calibration sources (filled circles) and simulated with the GEANT3 code (solid line). In addition, relative efficiencies deduced from a ^{56}Co source (open circles), from transitions in ^{11}B (open triangles) and ^{16}O (open square) adjusted to the calculated curve as described in the text are given. The drop of efficiency below 1 MeV is due to absorber foils in front of the detectors.

was normalized by adjusting the area of the full-energy peak at 15.110 MeV to the measured one. The comparison shows that the simulation describes the interaction of photons with the detector material sufficiently well and reproduces the measured spectrum within a few percent.

The absolute efficiency of the two HPGe detectors at 127° to the beam calculated by using GEANT3 is shown in Fig. 3. The absolute efficiency was determined experimentally up to 1332 keV from measurements of ^{22}Na, ^{60}Co, ^{133}Ba, and ^{137}Cs calibration sources. As shown in Fig. 3 experimental and simulated efficiencies agree well. An uncalibrated ^{56}Co source produced in-house using the ^{56}Fe$(p, n)^{56}$Co reaction was used to check the shape of the simulated efficiency curve up to 3.5 MeV. The relative efficiency values obtained from the ^{56}Co source were adjusted to the calculated value at 1238 keV and are consistent with the curve at higher energies (see Fig. 3).

The absolute photon flux was determined from intensities and the known integrated scattering cross section of transitions in ^{11}B, which was combined with the ^{88}Sr target (cf. Sec. II). For interpolation, the photon flux was calculated by using a code [25] based on the approximation given in Ref. [26] and including a screening correction according to Ref. [27]. This flux was corrected for absorption in the aluminum absorber placed behind the radiator and was then adjusted to the experimental values, as is shown in Fig. 4. Several approaches to the calculation of the photon flux are discussed and compared with the flux derived from a measurement of protons emitted during the dissociation of deuterons in Ref. [12]. It was shown that the various approaches reproduce the experiment well. Therefore, we used the calculated flux to determine the relative efficiency of the detectors at the energies of transitions with known integrated scattering cross sections. This was done for a measurement with a $H_3^{11}BO_3$ target. From

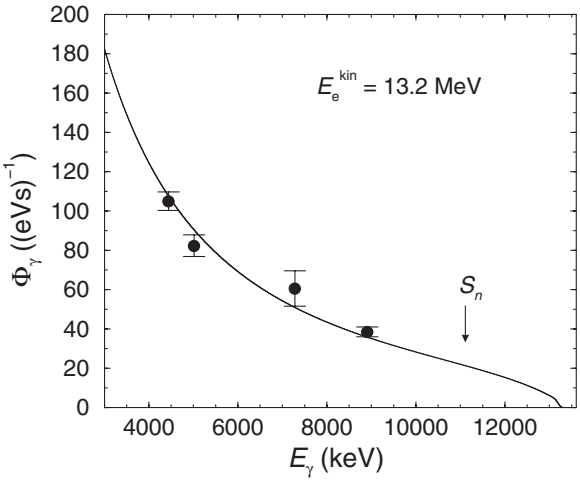

FIG. 4. Absolute photon flux at the target deduced from intensities of transitions in ^{11}B (circles) using the calculated efficiency shown in Fig. 3 and relative photon flux calculated as described in the text (solid line).

the intensities of transitions in ^{11}B and ^{16}O and the calculated photon flux we deduced values for the relative efficiency, which were adjusted to the calculated value of the photon flux at 4444 keV and are shown in Fig. 3. The values are in good agreement with the calculated efficiency curve and prove its shape up to 9 MeV.

C. Experiments at various electron energies

The measurements at various electron energies allow us to estimate the influence of feeding on the integrated cross sections. Ratios of the quantities I_{s+f} obtained for levels in ^{88}Sr from measurements at different electron energies are shown in Fig. 5. These ratios indicate to what extent the integrated cross sections are overestimated because of feeding transitions. The values of the integrated cross sections at $E_e^{\rm kin} = 6.8$ MeV were taken from Ref. [19]. The plotted ratios reveal that (i) only levels below $E_x \approx 6$ MeV are influenced considerably by feeding and (ii) the levels are mainly fed by levels above $E_x \approx 9$ MeV. This finding, in conjunction with the energies of the lowest lying state in ^{88}Sr [$E_x(2_1^+) \approx$ 1.8 MeV] and the highest lying state ($E_x \approx 12$ MeV), indicates that the energy of an inelastic transition depopulating a high-lying to a low-lying state that de-excites directly to the ground state (two-step cascade) is expected to be in the range from 3 to 10 MeV. If the inelastic transition populates another level in between, the energies of the transitions in this three-step cascade are correspondingly smaller. Transitions found in the measurement at $E_e^{\rm kin} = 6.8$ MeV are known to be ground-state transitions [19]. Transitions additionally observed up to 6.8 MeV in the measurements at 9.0 and 13.2 MeV are therefore considered as branchings from high-lying to low-lying excited states. In the same way, transitions in the range from 7 to 9 MeV observed in the measurement at 9.0 MeV are considered as ground-state transitions, whereas transitions in this energy range found additionally at 13.2 MeV are considered as branchings to low-lying states. By comparing

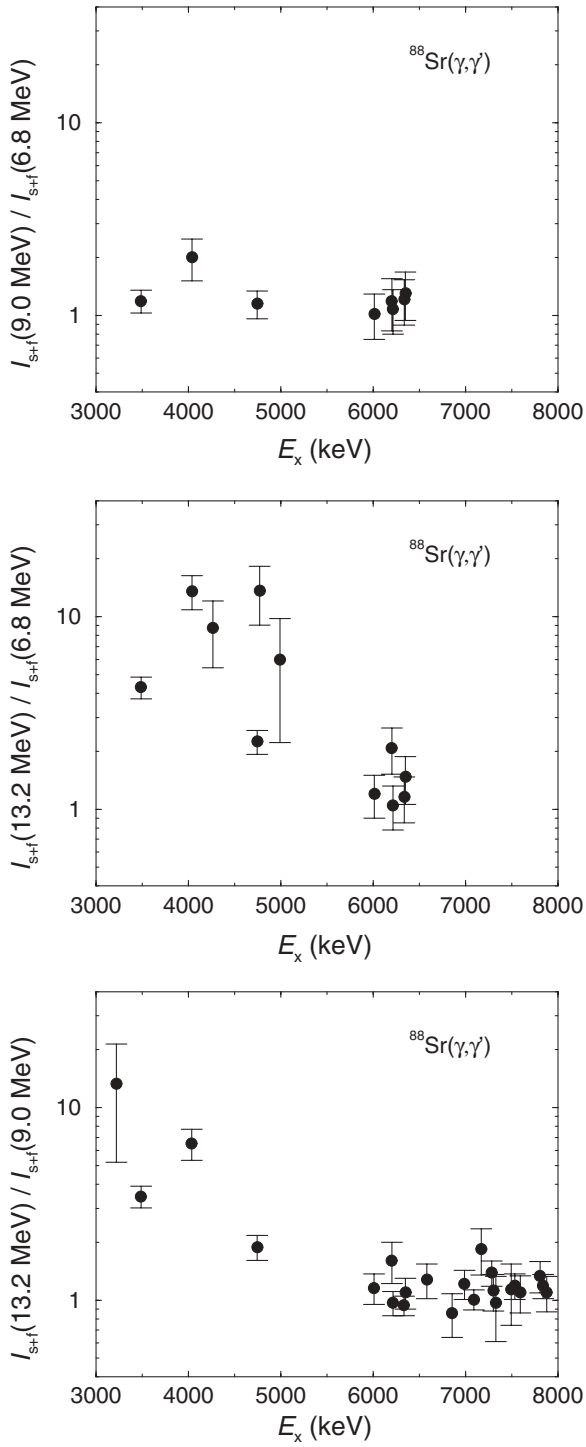

FIG. 5. Ratios of integrated cross sections I_{s+f} of transitions in ^{88}Sr obtained at different electron energies.

the measurements in this way, transitions from high-lying to excited low-lying states may be filtered out. The remaining transitions, assumed as ground-state transitions, have been used to derive the corresponding level energies, which are listed in Table I together with the multipolarities of the ground-state transitions deduced from angular distributions and polarizations (see Sec. II D), the integrated scattering cross sections, and the quantities Γ_0^2/Γ.

TABLE I. Levels assigned to ^{88}Sr.

E_x[a] (keV)	$\frac{\dot{N}_\gamma(90°)}{\dot{N}_\gamma(127°)}$[b]	$\frac{\dot{N}_{\gamma\parallel}-\dot{N}_{\gamma\perp}}{\dot{N}_{\gamma\parallel}+\dot{N}_{\gamma\perp}}$[c]	J_x^π[d]	$\frac{I_{s+f}(9.0)}{I_{s+f}(6.8)}$[e]	$\frac{I_{s+f}(13.2)}{I_{s+f}(6.8)}$[e]	$\frac{I_{s+f}(13.2)}{I_{s+f}(9.0)}$[e]	I_s[f] (eV b)	Γ_0^2/Γ[g] (meV)
1835.9(1)	1.26(11)	+0.047(5)	2^+[h]			10.0(13)	206(19)	60(6)
3218.3(1)	1.09(9)		2^+[h]			13(8)	10(6)	9(5)
3486.3(1)	0.83(6)	+0.096(16)	1^+[h]	1.2(2)	4.3(6)	3.5(5)	192(15)	202(16)
4035.6(1)	1.8(3)	+0.08(2)	2^+[h]	2.0(5)	14(3)	6.5(12)	52(8)	73(11)
4742.7(1)	0.91(9)		1^-[h]	1.2(2)	2.2(3)	1.9(3)	63(7)	123(14)
6008.9(2)	0.74(9)	−0.24(13)	1^-	1.0(3)	1.2(3)	1.2(2)	96(12)	354(34)
6200.6(2)	0.79(8)	+0.23(10)	1^+	1.2(4)	2.1(6)	1.6(4)	44(8)	147(27)
6212.1(1)	0.77(3)	−0.25(3)	1^-[h]	1.1(3)	1.0(3)	0.97(14)	591(43)	1978(144)
6333.4(1)	0.80(4)	−0.251(13)	1^-[h]	1.2(3)	1.2(3)	0.94(11)	885(65)	3078(226)
6346.4(2)	0.86(7)	−0.230(45)	1^-	1.3(4)	1.5(4)	1.1(2)	101(12)	353(42)
6591.7(9)	1.6(5)						23(6)	87(23)[i]
6854.6(3)	0.60(10)		1			0.9(2)	57(11)	232(45)
6987.9(2)	0.61(8)	−0.20(8)	1^-			1.2(2)	142(16)	601(48)
7089.1(1)	0.81(4)	−0.235(15)	1^-[h]			1.0(1)	963(72)	4197(314)
7169.2(2)	0.93(14)		1			1.8(5)	39(8)	174(36)
7281.8(3)	0.59(7)	−0.22(4)	1^-			1.4(2)	180(18)	828(83)
7299.9(3)	0.34(12)	−0.37(6)	$(1)^-$			1.1(2)	89(12)	411(55)
7492.8(3)	0.68(15)	−0.27(16)	1^-			1.1(4)	36(11)	175(54)
7533.9(2)	0.86(7)	−0.22(7)	1^-			1.2(2)	293(28)	1442(138)
7591.3(3)	0.72(10)	−0.25(11)	1^-			1.1(2)	99(15)	495(75)
7807.8(3)	0.79(7)	−0.27(7)	$1^{(-)}$			1.3(3)	161(23)	851(122)
7838.3(2)	0.78(6)	−0.08(4)	1^-[h]			1.2(2)	386(37)	2056(197)
7877.3(3)	0.27(12)	−0.37(2)	$(1)^-$			1.1(2)	130(22)	699(118)
7964.2(2)	0.77(6)	−0.12(7)	1^-				267(29)	1468(159)
7987.6(2)	0.79(7)	−0.13(8)	1^-				158(19)	874(105)
8040.8(1)	0.85(6)	−0.19(3)	1^-				581(62)	3257(348)
8109.5(3)	0.88(10)	−0.30(8)	1^-				147(24)	838(137)
8180.7(3)	0.83(9)	−0.15(4)	1^-				163(21)	946(122)
8191.1(2)	0.81(7)	−0.19(4)	1^-				238(28)	1385(163)
8215.3(2)	0.74(9)	−0.19(4)	1^-				220(26)	1287(152)
8271.5(3)	0.71(15)	−0.14(12)	1^-				143(25)	848(148)
8325.7(3)	0.79(9)	−0.13(6)	1^-				193(28)	1160(168)
8375.8(6)	0.47(17)		1				60(20)	365(122)
8403.0(4)	0.46(14)		1				99(21)	606(129)
8453.4(3)	0.67(5)	−0.28(9)	1^-				365(44)	2262(273)
8469.0(3)	0.74(9)	−0.22(14)	1^-				117(22)	728(137)
8500.8(3)	0.52(11)		1				211(32)	1322(200)
8518.8(4)	0.62(14)	−0.35(19)	1^-				108(24)	680(151)
8553.2(9)							43(13)	273(82)[i]
8561.3(6)							87(19)	553(121)[i]
8580.6(5)							70(17)	447(109)[i]
8588.7(4)							124(27)	793(173)[i]
8626.2(10)							53(15)	342(97)[i]
8668.6(6)	0.62(15)		1				56(10)	365(65)
8682.0(6)	0.6(3)		1				27(6)	176(39)
8713.7(9)	0.8(2)	−0.14(6)	1^-				115(68)	757(448)
8735.8(9)	1.20(17)						94(15)	622(99)[i]
8754.6(8)	0.75(12)		1				131(22)	871(146)
8764.7(5)							29(7)	193(47)[i]
8779.8(6)	0.95(19)						72(14)	481(94)[i]
8791.9(6)	0.58(12)		1				70(13)	469(87)
8840.1(4)	1.1(2)						107(21)	725(142)[i]

TABLE I. *(Continued.)*

E_x [a] (keV)	$\frac{\dot{N}_\gamma(90^\circ)}{\dot{N}_\gamma(127^\circ)}$ [b]	$\frac{\dot{N}_{\gamma\parallel}-\dot{N}_{\gamma\perp}}{\dot{N}_{\gamma\parallel}+\dot{N}_{\gamma\perp}}$ [c]	J_x^π [d]	$\frac{I_{s+f}(9.0)}{I_{s+f}(6.8)}$ [e]	$\frac{I_{s+f}(13.2)}{I_{s+f}(6.8)}$ [e]	$\frac{I_{s+f}(13.2)}{I_{s+f}(9.0)}$ [e]	I_s [f] (eV b)	Γ_0^2/Γ [g] (meV)
8850.6(12)							23(7)	156(48)[i]
8874.4(5)	0.8(3)		1				44(9)	300(61)
8928.5(3)	0.86(7)	−0.15(5)	1^-				323(38)	2232(263)
8980.8(6)	1.1(2)						97(17)	678(119)[i]
9019.2(6)							41(11)	289(78)[i]
9043.5(5)	0.69(14)	−0.11(10)	1^-				122(25)	865(177)
9069.7(6)	0.76(15)	−0.12(11)	1^-				105(18)	749(128)
9078.3(3)	0.87(14)	−0.12(10)	1^-				170(27)	1215(193)
9098.3(7)	0.7(2)		1				51(15)	366(108)
9116.3(5)	1.0(2)						121(20)	872(144)[i]
9125.11(3)	0.70(12)		1				187(26)	1350(188)
9148.3(2)	0.76(8)	−0.20(6)	1^-				343(41)	2489(298)
9191.3(2)	0.78(7)	−0.12(4)	1^-				378(46)	2769(337)
9214.4(7)	0.59(17)		1				85(16)	626(118)
9255.2(9)	0.6(3)		1				38(13)	282(97)
9305.2(3)	0.69(8)	−0.11(6)	1^-				387(57)	2905(428)
9341.1(3)	0.84(14)	−0.42(16)	1^-				109(19)	825(144)
9384.6(7)	0.77(12)		1				84(16)	641(122)
9393.3(5)	0.74(9)		1				141(23)	1079(176)
9402.4(5)	0.74(9)		1				108(18)	828(138)
9431.8(10)	0.81(17)		1				102(21)	787(162)
9445.5(4)	0.84(9)	−0.17(5)	1^-				361(50)	2793(387)
9470.5(4)	1.08(16)	−0.29(14)	(1^-)				226(33)	1757(257)
9478.7(5)	0.78(14)	−0.19(13)	$1^{(-)}$				140(23)	1091(179)
9497.1(2)	0.90(9)	−0.17(3)	1^-				558(60)	4363(469)
9550.8(7)	1.0(4)						51(16)	403(127)[i]
9568.3(5)	0.79(13)		1				131(25)	1040(198)
9576.8(11)							48(13)	382(103)[i]
9597.9(11)	0.6(2)		1				51(13)	407(104)
9616.3(6)	0.88(18)		1				105(20)	842(160)
9646.1(8)			1				32(9)	258(73)
9704.1(5)	0.77(10)	−0.17(8)	1^-				245(46)	2001(376)
9728.1(18)							24(11)	197(90)[i]
9738.1(16)	0.9(2)		1				76(20)	625(164)
9746.0(6)	0.64(12)	−0.160(77)	1^-				301(52)	2479(428)
9804.7(9)	0.8(2)		1				52(13)	433(108)
9816.5(3)	0.56(10)	−0.31(6)	1^-				141(24)	1178(201)
9881.2(4)	0.88(10)	−0.21(12)	$1^{(-)}$				205(31)	1735(262)
9944.1(8)	0.65(16)	−0.30(11)	1^-				116(20)	995(171)
9953.3(5)							164(26)	1409(223)[i]
9965.8(6)	0.85(18)	−0.13(12)	$1^{(-)}$				102(17)	878(146)
10056.3(4)	0.73(15)		1				86(14)	754(123)
10089.2(10)							34(11)	300(97)[i]
10106.9(8)	0.63(14)		1				60(16)	531(142)
10128.2(7)							55(12)	489(107)[i]
10139.5(8)							48(11)	428(98)[i]
10150.3(8)							58(16)	518(143)[i]
10184.0(4)							14(4)	126(36)[i]
10248.6(4)	0.62(14)		1				31(8)	282(73)
10288.6(7)	0.64(14)	−0.22(11)	$1^{(-)}$				110(23)	1009(211)
10297.7(13)							47(11)	432(101)[i]

TABLE I. *(Continued.)*

E_x [a] (keV)	$\frac{\dot{N}_\gamma(90^\circ)}{\dot{N}_\gamma(127^\circ)}$ [b]	$\frac{\dot{N}_{\gamma\parallel}-\dot{N}_{\gamma\perp}}{\dot{N}_{\gamma\parallel}+\dot{N}_{\gamma\perp}}$ [c]	J_x^π [d]	$\frac{I_{s+f}(9.0)}{I_{s+f}(6.8)}$ [e]	$\frac{I_{s+f}(13.2)}{I_{s+f}(6.8)}$ [e]	$\frac{I_{s+f}(13.2)}{I_{s+f}(9.0)}$ [e]	I_s [f] (eV b)	Γ_0^2/Γ [g] (meV)
10326.6(6)							26(7)	240(75)[i]
10341.2(6)							29(10)	269(93)[i]
10372.5(5)							101(85)	942(793)[i]
10406.6(14)							143(98)	1343(920)[i]
10421.1(10)							64(55)	603(518)[i]
10453.2(12)							37(14)	351(133)[i]
10481.1(9)	1.5(6)						42(13)	400(124)[i]
10512.1(19)	1.1(3)						62(18)	594(172)[i]
10522.7(5)	0.64(10)		1				264(45)	2534(432)
10550.3(5)	0.56(19)		1				119(20)	1148(193)
10600.2(16)							77(22)	749(214)[i]
10608.7(14)	1.2(3)						115(30)	1122(293)[i]
10644.1(8)	0.89(19)	−0.29(6)	1^-				156(33)	1532(324)
10657.8(16)	0.9(2)		1				124(38)	1221(374)
10698.4(8)							37(11)	367(109)[i]
10726.4(15)	0.6(3)		1				57(22)	569(219)
10744.9(8)							57(16)	571(160)[i]
10759.7(16)	1.3(3)						46(13)	462(131)[i]
10767.1(15)	0.8(2)		1				63(24)	633(241)
10783.6(5)	0.84(13)		1				244(50)	2460(504)
10804.7(6)	1.1(3)						107(38)	1083(385)[i]
10857.2(6)	1.5(5)						26(7)	266(72)[i]
10888.3(13)							66(22)	678(226)[i]
10914.6(5)	0.76(18)		1				127(24)	1312(248)
10929.9(7)	1.1(3)						88(20)	911(207)[i]
10950.4(6)							101(20)	1050(208)[i]
10979.7(12)							47(18)	491(188)[i]
11012.0(5)	0.66(10)		1				223(36)	2345(378)
11059.0(11)							57(18)	605(191)[i]
11083.0(11)							57(19)	607(202)[i]
11111.8(16)	0.7(2)		1				80(26)	856(278)
11125.4(14)	0.7(2)		1				88(28)	1052(354)
11169.5(12)							50(15)	541(162)[i]
11224.2(13)							43(21)	470(229)[i]
11251.8(12)							61(19)	669(208)[i]
11278.9(10)	0.66(17)		1				136(31)	1500(342)
11313.8(6)							185(109)	2053(1210)[i]
11326(3)							19(7)	211(78)[i]
11335.3(13)	0.51(13)		1				369(135)	4111(1504)
11355(3)							273(138)	3052(1543)[i]
11370(3)	0.72(18)		1				287(100)	3217(1121)
11393.6(6)	0.49(18)		1				54(13)	608(146)
11413.2(15)							43(20)	486(226)[i]
11548.0(7)							20(6)	231(69)[i]
11593.7(16)							23(8)	268(93)[i]
11607.6(12)							32(9)	374(105)[i]
11633.0(14)							23(7)	270(82)[i]
11658.0(16)							18(7)	212(82)[i]
11743.1(14)							29(10)	347(120)[i]
11782.4(14)							26(10)	313(120)[i]
11920.6(7)							31(8)	382(99)[i]
11935.5(10)							17(6)	210(74)[i]

TABLE I. *(Continued.)*

E_x [a] (keV)	$\frac{\dot{N}_\gamma(90^\circ)}{\dot{N}_\gamma(127^\circ)}$ [b]	$\frac{\dot{N}_{\gamma\parallel}-\dot{N}_{\gamma\perp}}{\dot{N}_{\gamma\parallel}+\dot{N}_{\gamma\perp}}$ [c]	J_x^π [d]	$\frac{I_{s+f}(9.0)}{I_{s+f}(6.8)}$ [e]	$\frac{I_{s+f}(13.2)}{I_{s+f}(6.8)}$ [e]	$\frac{I_{s+f}(13.2)}{I_{s+f}(9.0)}$ [e]	I_s [f] (eV b)	Γ_0^2/Γ [g] (meV)
11958.9(14)							9(4)	112(50) [i]
12026.5(10)							18(6)	226(75) [i]

[a]Excitation energy. The error in parentheses is given in units of the last digit. This energy was deduced from the γ-ray energy measured at 127° to the beam by including a recoil and Doppler correction.
[b]Ratio of the rates of the ground-state transitions measured at angles of 90° and 127°. The expected values for an elastic pure-dipole transition (spin sequence 0–1–0) and for an elastic quadrupole transition (spin sequence 0–2–0) are 0.74 and 2.22, respectively. If the transition were a cascade transition fed by one level above, one would expect the following ratios when assuming pure transitions: 1.0 for spin sequence 0–1–1–0, 1.0 for spin sequence 0–1–2–0, 1.14 for spin sequence 0–2–2–0, and 1.0 for spin sequence 0–2–1–0.
[c]Azimuthal asymmetry of the ground-state transitions deduced from the scattering of polarized photons. The criterion for a definite parity assignment is that the considered value fits one of the dashed bands shown in Fig. 8 within its error bars and is by at least twice the error apart from the band of the other parity.
[d]Spin and parity of the state.
[e]Ratio of integrated scattering + feeding cross sections deduced at different electron energies. The deviation from unity is a measure of feeding. The values of I_{s+f} at $E_e^{\rm kin} = 6.8$ MeV were taken from Ref. [19].
[f]Integrated scattering cross section. The values up to the level at 7877 keV were deduced from the measurement at $E_e^{\rm kin} = 9.0$ MeV; the values given for levels at higher energies were deduced from the measurement at $E_e^{\rm kin} = 13.2$ MeV.
[g]Partial width of the ground-state transition Γ_0 multiplied by the branching ratio $b_0 = \Gamma_0/\Gamma$. An estimate of the partial width Γ_0 can be obtained from Γ_0^2/Γ after correction for a mean branching ratio $b_0 = \Gamma_0/\Gamma = 85(15)\%$ for resolved ground-state transitions (cf. Table II and Sec. III), leading to a correction factor of 1.18(21). For transitions in the energy range between 6 and 9 MeV a possible remaining feeding of 10(5)% as deduced from the ratios $I_{s+f}(13.2)/I_{s+f}(9.0)$ has also to be taken into account, which leads together with the branching ratio to an effective correction factor of 0.94(17).
[h]Spin and parity have been known from previous work (cf. Sec. I).
[i]Value deduced under the assumption of $J_x = 1$.

The detection limit, defined as twice the statistical error of the area of a background window with the FWHM of a peak observed at the considered energy, is shown in terms of Γ_0 in Fig. 6 for the measurements at the three electron energies.

In general, the complete level scheme may be constructed by searching for combinations of γ-ray energies that fit another γ ray according to the Ritz principle. However, if one includes all observed transitions one finds a huge number of possible two-fold or even three-fold combinations. For instance, one obtains about 1600 two-fold combinations, including mainly transitions in the range of 3–6 MeV at an uncertainty of the transition energy of 0.5 keV. For feeding transitions with energies greater than 6 MeV that do not match any energies of ground-state transitions one obtains the two-fold combinations listed in Table II. All these combinations include inelastic transitions to the low-lying 2^+ and 1^+ states below about 4 MeV. The ratios Γ_{2^+}/Γ_0 given in Table II are compatible with the ratios of cross sections of inelastic scattering to the first 2^+ state and of elastic scattering deduced from experiments with monoenergetic photons [8].

Since we cannot derive complete information about the many possible branching transitions, we are unable to determine the branching ratios of the ground-state transitions from the present data. Therefore, other methods have to be applied

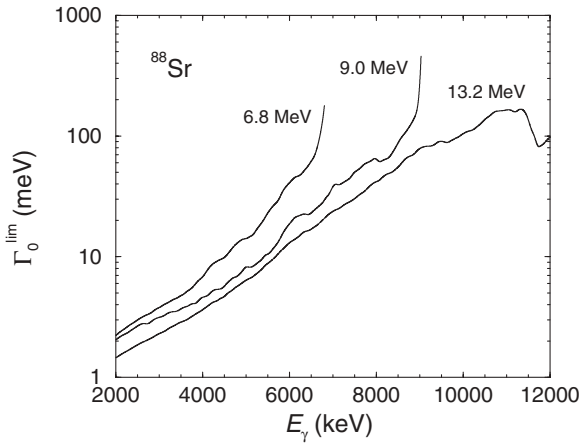

FIG. 6. Detection limits for resolved peaks in the measurements at 6.8, 9.0, and 13.2 MeV (see text).

TABLE II. High-energy inelastic transitions to low-lying 2^+ and 1^+ states in ^{88}Sr.

$E_{\gamma 0}$ (keV) [a]	$E_{\gamma f}$ (keV) [b]	$E_{\gamma c}$ (keV) [c]	Γ_f/Γ_0 [d]
11167.1	7681.9	3486.0	0.35(15)
11080.6	7861.7	3217.9	0.26(11)
10885.4	7667.3	3217.9	0.33(14)
10855.4	7368.1	3486.0	0.52(18)
10802.9	8966.4	1835.7	0.26(11)
9477.6	7642.0	1835.7	0.14(4)
9189.6	7352.9	1835.7	0.16(3)
9041.6	7205.4	1835.7	0.29(8)

[a]Energy of the elastic (ground-state) transition.
[b]Energy of the inelastic transition.
[c]Energy of the cascade transition depopulating the low-lying state to the ground state.
[d]Ratio of the partial widths of the inelastic and elastic transitions.

to correct the dipole-strength distribution for branching ratios (see Sec. III).

D. Experiment with polarized photons

To determine the linear polarization of γ transitions we performed a photon-scattering experiment with polarized photons. Using two steering magnets the electron beam was deflected from the normal direction and then deflected back such that it hits the radiator in the center under a selected angle. As a consequence, an off-axis portion of the spatial distribution of the photons, which is partly polarized, is transmitted through the fixed collimator. The deflection angle for the production of polarized bremsstrahlung was chosen as $\theta = m_0c^2/E_e$, the ratio of the rest energy to the full energy of the electron, where a maximum degree of polarization is expected [28]. The steering magnets were designed such that the electron beam can be deflected to four azimuthal angles of $\phi = 0°$, 90°, 180°, and 270°, thus defining four different planes of polarization. A cyclical use of these four directions enabled us to reduce the influence of fluctuations of the beam alignment and of uncertainties of, for example, the steerer adjustments.

The degree of polarization was measured via the photodisintegration of the deuteron. Predominant $E1$ absorption above 4 MeV causes the emission of protons preferentially in the direction of the electric field vector of the polarized bremsstrahlung. The degree of polarization can be deduced from azimuthal asymmetries of the intensities of the protons, which were measured with four silicon detectors placed at polar angles of $\theta = 90°$ relative to the photon beam and at azimuthal angles of $\phi = 0°$, 90°, 180°, and 270°, respectively. A polyethylene film of an areal density of 4 mg/cm^2, in which hydrogen is substituted by deuterium (CD2), was used as a target. The CD2 film was positioned parallel to the incident beam such that it was observed by all four detectors under 45°. Further details of the setup are given in Ref. [12].

The present experiment was carried out at a kinetic electron energy of 16 MeV with a measuring time of 200 h. The degree of polarization P_γ was deduced from azimuthal asymmetries $P_\gamma \Sigma(\theta) = (\dot{N}_{p\parallel} - \dot{N}_{p\perp})/(\dot{N}_{p\parallel} + \dot{N}_{p\perp})$, where $\dot{N}_{p\parallel}$ and $\dot{N}_{p\perp}$ are the rates of protons resulting from the disintegration of deuterons and measured perpendicular or parallel to the polarization plane, respectively, and $\Sigma(\theta) = [W(\theta, \phi = 0°) - W(\theta, \phi = 90°)] / [W(\theta, \phi = 0°) + W(\theta, \phi = 90°)]$ is the analyzing power, which is close to unity at an emission angle of $\theta = 90°$ and the chosen geometry. The degree of polarization as deduced for the present experiment is shown in Fig. 7. Spectra measured with those detectors, which belong to the same orientation relative to the polarization plane, were added up. The energies of the protons were rescaled to the energies of the incident photons according to $E_\gamma = E_p + E_n + E_B$, where E_γ is the energy of the incident photon, $E_p \approx E_n$ are the kinetic energies of the proton and neutron, respectively, and $E_B = 2225$ keV is the binding energy of the deuteron. Asymmetries deduced for transitions in ^{88}Sr as $(\dot{N}_{\gamma\parallel} - \dot{N}_{\gamma\perp})/(\dot{N}_{\gamma\parallel} + \dot{N}_{\gamma\perp})$, where $\dot{N}_{\gamma\parallel}$ and $\dot{N}_{\gamma\perp}$ are the rates of γ transitions observed parallel or perpendicular to the polarization plane, respectively, are given in Table I. The values obtained for the transitions at 1836, 3486, and 4035 keV are consistent with the parities known for the respective states but are attenuated by feeding. The values deduced for the transitions at 6212, 6333, 7088, 7837, and 8040 keV are consistent with those given in previous work [17]. The asymmetries of the transitions with energies greater than 6 MeV are depicted in Fig. 8. Except for the transition at 6201 keV, all transitions above 6 MeV are $E1$ transitions. The transitions, which have been proven as $E1$ transitions, include 63% of the total dipole strength found for all transitions in the range from 6 to 12 MeV (cf. Table I).

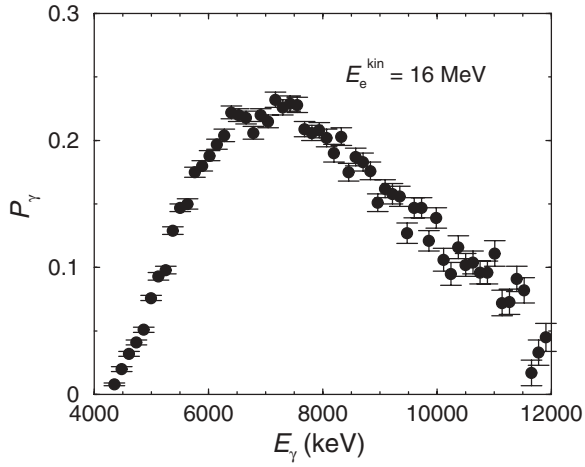

FIG. 7. Degree of polarization as a function of the photon energy as deduced from spectra of protons emitted from disintegrated deuterons. Data below $E_\gamma \approx 7$ MeV do not reflect the real behavior because of the contamination of the proton spectra with scattered photons and secondary electrons below about 2.5 MeV. The degree of polarization is expected to increase further toward low energies with the slope observed above 7 MeV.

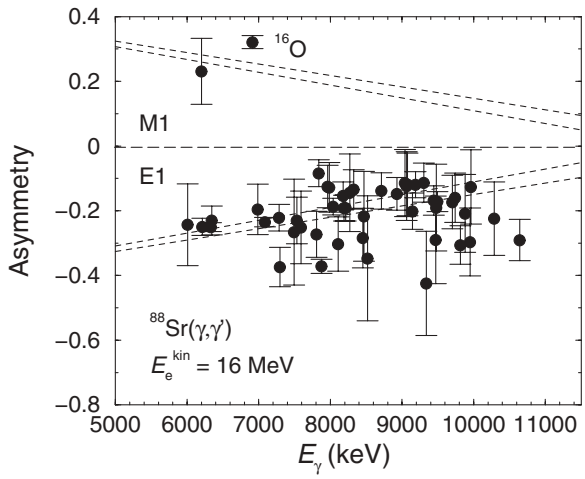

FIG. 8. Experimental asymmetries $(\dot{N}_{\gamma\parallel} - \dot{N}_{\gamma\perp})/(\dot{N}_{\gamma\parallel} + \dot{N}_{\gamma\perp})$ of γ rays in ^{88}Sr. The bands marked with dashed lines indicate the degree of polarization as derived from Fig. 7. The data point marked ^{16}O belongs to a known $E2$ transition arising from the oxygen in the $^{88}SrCO_3$ target.

III. DETERMINATION OF THE DIPOLE-STRENGTH DISTRIBUTION

To deduce the correct dipole-strength distribution, inelastic transitions have to be sorted out and the ground-state transitions have to be corrected for their branching ratios b_0. As explained in Sec. II C a definite and complete assignment of branching transitions to particular levels is not possible. Therefore we will use statistical methods to estimate the contributions of branching transitions and of the branching ratios of the ground-state transitions.

By using simulations as described in Sec. II B we corrected the spectrum including the two detectors at 127°, measured during the irradiation of the ^{88}Sr target at $E_e^{\mathrm{kin}} = 13.2$ MeV. In a first step spectra of the ambient background adjusted to the intensities of the 1460.5-keV transition (decay of ^{40}K) and 2614.9-keV transition (decay of ^{208}Tl) in the in-beam spectrum were subtracted from the measured spectrum. It turned out that transitions following (n, γ) reactions in the HPGe detectors and in surrounding materials are negligibly small and thus did not require correction. To correct the spectrum for detector response, spectra of monoenergetic γ rays were calculated in steps of 10 keV by using GEANT3. Starting from the high-energy end of the experimental spectrum, the simulated spectra were subtracted sequentially. The resulting spectrum including the two detectors at 127° is shown in Fig. 9. The background produced by atomic processes in the ^{88}Sr target was obtained from a GEANT3 simulation using the absolute photon flux deduced from the intensities of the transitions in ^{11}B (cf. Fig. 4). The corresponding background spectrum multiplied with the efficiency curve shown in Fig. 3 and with the measuring time is also depicted in Fig. 9. As can be seen in Fig. 9 the continuum in the spectrum of photons scattered from ^{88}Sr is clearly higher than the background by atomic scattering. This continuum may be formed by a large number of nonresolvable transitions with small intensities; these are a consequence of the increasing nuclear level density at high energy and of Porter-Thomas fluctuations of the decay

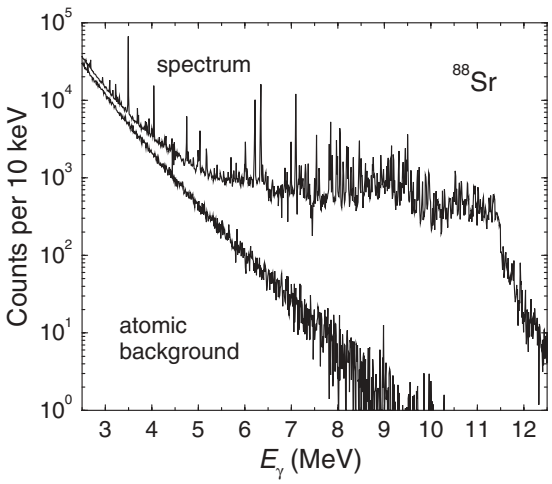

FIG. 9. Experimental spectrum of ^{88}Sr (corrected for room background and detector response) and simulated spectrum of atomic background (multiplied by efficiency and measuring time).

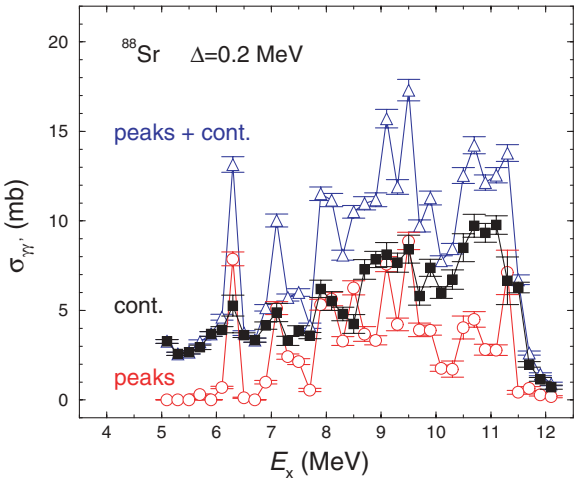

FIG. 10. (Color online) Scattering cross sections in ^{88}Sr, derived as $\sigma_{\gamma\gamma'} = \sum_\Delta I_s/\Delta$, not corrected for branching and averaged over energy bins of $\Delta = 0.2$ MeV, as derived from the difference of the experimental spectrum and the atomic background shown in Fig. 9 ("peaks + cont."; open blue triangles) and from the resolved peaks only ("peaks"; open red circles). In addition, the results of subtracting the values of the peaks from the spectrum that represent the continuum contribution ("cont."; black filled boxes) are shown.

widths [29] in connection with the finite detector resolution (e.g., $\Delta E \approx 7$ keV at $E_\gamma \approx 9$ MeV).

The relevant intensity of the photons resonantly scattered from ^{88}Sr is obtained from a subtraction of the atomic background from the response-corrected experimental spectrum. The remaining intensity distribution includes the intensity contained in the resolved peaks as well as the intensity of the "nuclear" continuum. The scattering cross sections $\sigma_{\gamma\gamma'}$ derived for energy bins of 0.2 MeV from the full intensity distribution are shown in Fig. 10. These values are compared with those given in Table I for resolved transitions in ^{88}Sr. One sees that the two curves have similar structures caused by the prominent peaks. However, the curve including also the continuum part of the spectrum contains altogether a strength that is by a factor of about 2.3 greater than the strength of the resolved peaks only. To illustrate the contribution of the continuum, the difference of the two curves is also shown. In this curve representing the continuum only, the peak structures are washed out, thus proving that these structures are caused by the resolved peaks. The full intensity distribution (resolved peaks and continuum) and the corresponding scattering cross sections shown in Fig. 10 contain ground-state transitions and, in addition, branching transitions to lower lying excited states (inelastic transitions) as well as transitions from those states to the ground state (cascade transitions). The different types of transitions cannot be clearly distinguished. However, for the determination of the photoabsorption cross section and the partial widths Γ_0 the intensities of the ground-state transitions are needed. Therefore, contributions of inelastic and cascade transitions have to be subtracted from the spectra. We corrected the intensity distributions by simulating γ-ray cascades [30] from the levels in the whole energy range analogously to the strategy of the Monte Carlo code DICEBOX [31]. In these

simulations, 1000 level schemes (nuclear realizations) starting from the ground state were created with level densities derived from the experiment [32]. We apply the statistical methods also for the low-energy part of the level scheme instead of using experimentally known low-lying levels in ^{88}Sr because this would require knowledge of the partial decay widths of all transitions populating these fixed levels. Fluctuations of the nearest-neighbor spacings were taken into account according to the Wigner distribution (see, e.g., Ref. [33]). The partial widths of the transitions to low-lying levels were assigned by using a priori known strength functions for $E1$, $M1$, and $E2$ transitions. Fluctuations of the partial widths were treated by applying the Porter-Thomas distribution [29].

The calculations used the recently published parameters for the back-shifted Fermi-gas model obtained from fits to experimental level densities [32], $a = 8.95(41)$ MeV^{-1} and $E_1 = 1.97(30)$ MeV. In the individual nuclear realizations, the values of a and E_1 were varied within their uncertainties. The resulting mean values of the level densities of all nuclear realizations for $J = 1$ states in ^{88}Sr are plotted in Fig. 11. We assumed equal level densities for states with positive and negative parities at the same spin. This assumption has been recently justified by an investigation of level densities in the energy range from 5 to 10 MeV by using the ^{90}Zr(^{3}He,t) reaction [34]. For comparison, the density of the resolved levels given in Table I is also shown in Fig. 11. The increasing discrepancy between the two curves toward high energies supports the conclusion that the continuum in the experimental spectrum is formed by unresolved peaks (see the previous discussion).

For the $E1, M1$, and $E2$ photon strength functions, Lorentzian parametrizations [35] were used. The parameters of the Lorentzian for the $E1$ strength were determined from a fit to (γ, n) data [21,22] in the energy range from 13 to

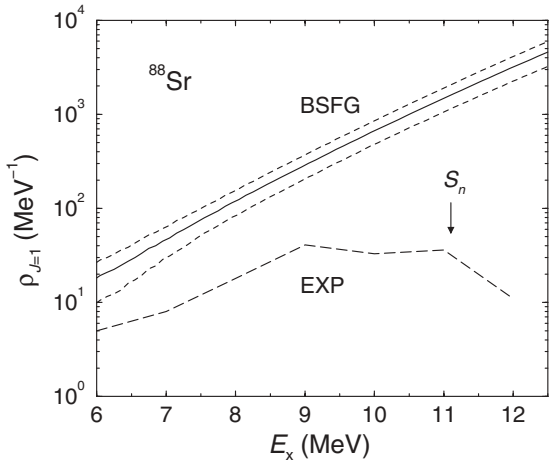

FIG. 11. Level density for $J = 1$ states in ^{88}Sr as a function of the excitation energy, calculated according to the back-shifted Fermi-gas model with the parameters given in Ref. [32] (BSFG) and level density derived from the levels given in Table I (EXP). The solid BSFG line represents the mean value over 1000 nuclear realizations; the dashed lines show the uncertainty of the mean values caused by the variation of the parameters a and E_1 used in the individual nuclear realizations and by fluctuations in the level spacings.

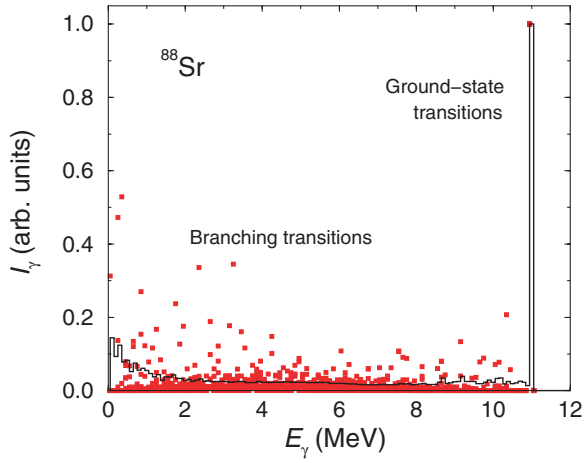

FIG. 12. (Color online) Simulated intensity distribution of transitions depopulating levels in a 100-keV bin around 11 MeV. The black line represents the mean distribution of 1000 nuclear realizations. The red squares depict the intensities obtained in 10 individual nuclear realizations.

18 MeV. The obtained parameters are energy of the maximum, $E_0 = 16.81(2)$ MeV, width $\Gamma = 4.0(1)$ MeV, and cross section at the maximum, $\sigma_0 = 206(2)$ mb. Note that the parameters σ_0 and Γ are consistent with the Thomas-Reiche-Kuhn sum rule [36], resulting in $\frac{\pi}{2}\sigma_0\Gamma = 60\,NZ/A$ MeV mb. The parameters for the $M1$ and $E2$ strengths were taken from global parametrizations of $M1$ spin-flip resonances and $E2$ isoscalar resonances, respectively [37].

Spectra of γ-ray cascades were generated for groups of levels in 100-keV bins in each of the 1000 nuclear realizations. For illustration, a mean intensity distribution of 1000 nuclear realizations including transitions depopulating levels in a 100-keV bin around 11 MeV is shown in Fig. 12 together with the distributions resulting from 10 individual nuclear realizations, which reflect the influence of fluctuations of level energies and level widths. Because in the nuclear realizations the levels were created randomly starting from the ground state instead of starting with the known first excited state at 1.8 MeV, the distribution of the branching transitions continues to the energy bin of the ground-state transitions. These spectra resemble qualitatively the ones measured in an experiment on ^{90}Zr using tagged photons [10]. Starting from the high-energy end of the experimental spectrum, which contains ground-state transitions only, the simulated intensities of the ground-state transitions were normalized to the experimental ones in the considered bin and the intensity distribution of the branching transitions was subtracted from the experimental spectrum. Applying this procedure step by step for each energy bin moving toward the low-energy end of the spectrum one obtains the intensity distribution of the ground-state transitions. Simultaneously, the branching ratios b_0^Δ of the ground-state transitions are deduced for each energy bin Δ. In an individual nuclear realization, the branching ratio b_0^Δ is calculated as the ratio of the sum of the intensities of the ground-state transitions from all levels i to the total intensity of all transitions depopulating all levels i in Δ to any low-lying

levels including the ground state:

$$b_0^{\Delta} = \frac{\sum_i \dot{N}_{\gamma i}^{\text{g.s.}}}{\sum_i \dot{N}_{\gamma i}^{\text{all}}} = \frac{\sum_i \Gamma_{0i}^2/\Gamma_i}{\sum_i \Gamma_{0i}}. \quad (3)$$

The second equivalence in Eq. (3) is based on Eqs. (1) and (2) and makes use of the fact that the sum of the intensities of all de-excitating transitions of a level i is equal to the total intensity of all excitations to this level. Note that b_0^{Δ} is not equivalent to an average over branching ratios as used for resolved transitions $\langle b_0 \rangle = \langle \Gamma_0/\Gamma \rangle$. Dividing the summed intensities in a bin of the experimental intensity distribution of the ground-state transitions by the corresponding branching ratio [Eq. (3)] we obtain the absorption cross section for a bin as $\sigma_\gamma^{\Delta} = \sigma_{\gamma\gamma}^{\Delta}/b_0^{\Delta}$. Finally, the absorption cross sections of each bin were obtained by averaging over the values of the 1000 nuclear realizations. For the uncertainty of the absorption cross section a 1σ deviation from the mean has been taken.

To get an impression of the branching ratios, the mean distribution of the calculated branching ratios b_0^{Δ} of 1000 nuclear realizations is shown in Fig. 13 together with the individual values of 10 nuclear realizations. The mean branching ratio decreases from about 80% for low-lying states, where only few possibilities for transitions to lower lying states exist, to about 65% at the neutron-separation energy. Toward low energy the uncertainty of b_0^{Δ} increases owing to level-spacing fluctuations and the decreasing level density. The large fluctuations below about 6 MeV make these values useless.

A possible problem of the described simulation may be the application of Porter-Thomas fluctuations to energy bins that contain resolved peaks corresponding to the most intense transitions in Table I. An analysis of the normalized distribution of the reduced level widths over their average $x = \Gamma_0 E^{-3}/\langle \Gamma_0 E^{-3} \rangle$ shows indeed deviations from the Porter-Thomas distribution $P(x) = (\sqrt{2\pi x})^{-1} e^{-x/2}$ for the strongest transitions. Therefore, as an alternative to the treatment of the full experimental intensity distribution, we have removed the intensities of the 14 most intense ground-state transitions given in Table I from the respective bins of the experimental intensity distribution. These 14 transitions represent 33% of the total of all scattering cross sections given in Table I. Then we applied the statistical analysis for the remaining distribution only. The full absorption cross sections were obtained by adding the scattering cross sections of the 14 levels to the absorption cross sections of the respective bins of the reconstructed distribution. This procedure is based on the assumption that the scattering cross sections of the 14 levels are nearly equal to the absorption cross sections (i.e. the branching ratios b_0 are close to one). The absorption cross sections deduced from the described reconstruction of either the full intensity distribution or from the separate treatment of the 14 most intense ground-state transitions in combination with the reconstruction of the remaining distribution are shown in Fig. 14. As can be seen at the bins including the prominent peaks (e.g., at the bins around 6.25, 6.35, 7.05, 7.85, 9.15, 9.35, and 9.45 MeV), the cross sections with the extra treatment of these peaks are lower than those of the treatment of the full distribution but overlap within their uncertainties. Note that the cross sections of the extra peaks taken from Table I are not corrected for branching ratios. Taking into account branching ratios of $b_0 \approx 0.8$–0.9, which are likely, for example, for intense peaks around 9 MeV (cf. Table II), we obtain cross sections from the extra treatment of the intense peaks that increase and come closer to the values obtained from the treatment of the full intensity distribution. For bins not containing the most intense peaks the results of the two different treatments are very close, which proves that a separate treatment of resolved peaks is necessary for the most intense peaks only. The small differences also imply that in the simulations of the γ-ray cascades the branching ratios produced for transitions with large partial widths Γ_0 exceed the mean values over all simulated transitions (see Fig. 13) considerably. To check this we recorded in the simulation the branching ratios calculated for all ground-state transitions with

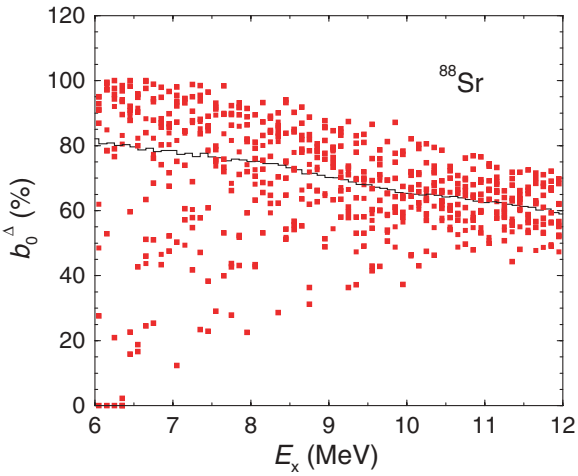

FIG. 13. (Color online) Branching ratios of ground-state transitions as obtained from the simulations of γ-ray cascades for ^{88}Sr. The solid line represents the mean distribution of 1000 nuclear realizations. The red squares represent the values of 10 individual nuclear realizations.

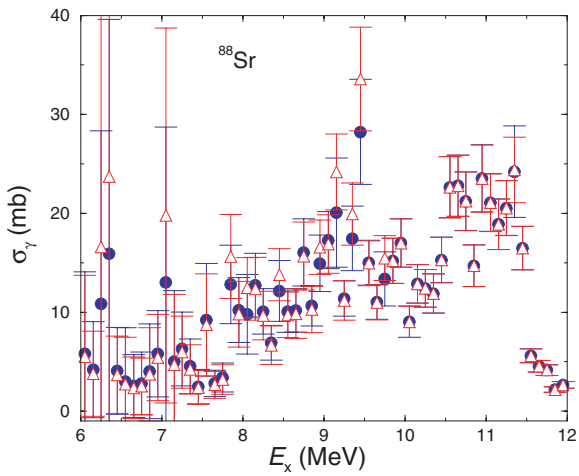

FIG. 14. (Color online) Cross sections deduced from the present (γ, γ') data for ^{88}Sr after correction for branching transitions. Red open triangles show the result of the correction of the full intensity distribution. Blue circles show the result of an extra treatment of the 14 strongest resolved peaks (see text).

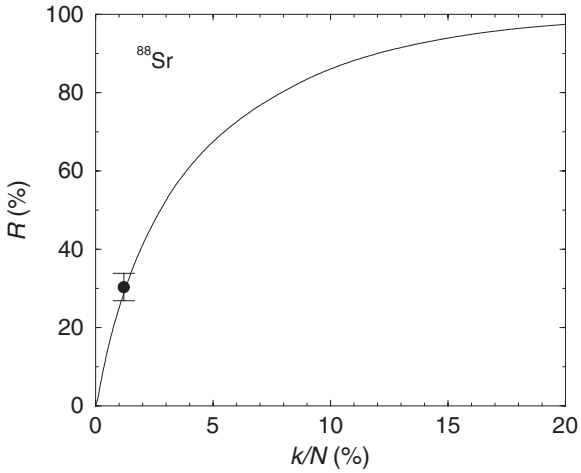

FIG. 15. Ratio $R = \sum_i^k I_{si} / \sum_i^N I_{si}$ of the sum of the k largest scattering cross sections of levels to the respective sum for all N levels in the energy range from 11 to 12 MeV as a function of the ratio of the number of levels k to the number of levels N. The solid line was deduced from the present simulations of γ-ray cascades; the data point was deduced from the present experiments (see text).

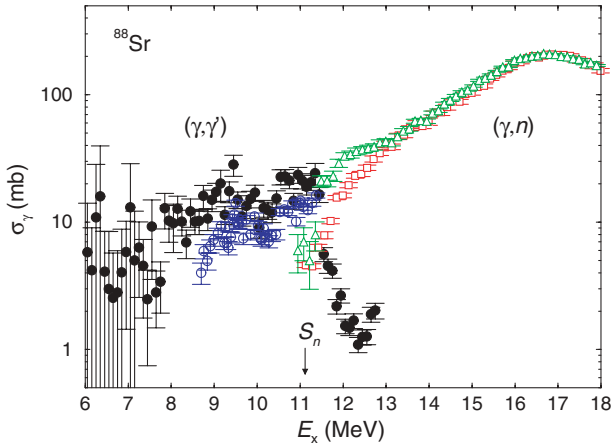

FIG. 16. (Color online) Photoabsorption cross sections deduced from the present photon-scattering data for ^{88}Sr according to $\sigma_\gamma = \sigma_{\gamma\gamma}/b_0$ after correction for branching transitions (filled black circles) in comparison with data obtained from an experiment with monoenergetic photons (open blue circles) [8] and with photoabsorption cross sections obtained from (γ, n) experiments as taken from Ref. [21] (open green triangles) and Ref. [22] (open red squares).

Γ_0 greater than the detection limits shown in Fig. 6 and found that these branching ratios have values of $b_0 \approx 0.85$–0.99, which is compatible with these findings. A further test of the correct treatment of intense peaks in the correction of the full intensity distribution is given in Fig. 15. This plot shows the ratio of the sum of the k greatest integrated cross sections of $J = 1$ levels generated in the energy bin from 11 to 12 MeV to the sum of the integrated cross sections of all N generated $J = 1$ levels in this energy bin. One sees, for example, that the levels with the greatest integrated cross sections, amounting to 5% of all levels, comprise almost 70% of the total integrated cross section of all levels in this energy range. The calculated curve fits well the experimental value deduced from the sum of the integrated cross sections of the $k = 26$ resolved levels between 11 and 12 MeV and the total integrated cross section deduced from the full intensity distribution (cf. Table I and Fig. 10) in this bin by using the number $N = 2200$ of all levels, as predicted by the BSFG model (cf. Fig. 11).

The photoabsorption cross sections obtained for ^{88}Sr are shown in Fig. 16 together with the data of a previous experiment with monoenergetic photons in the energy range from 8.6 to 12 MeV [8] and with the data of (γ, n) experiments [21,22]. The cross section of the (γ, p) reaction is very small in the considered energy range [38] and was neglected. The photoabsorption cross sections obtained from the present (γ, γ') experiments after the described correction are consistent with the cross sections obtained from the experiment with monoenergetic photons [8]. The comparison of the present data with (γ, n) data shows a smooth connection between the data of the two different experiments. Consequently, the present (γ, γ') data provide new information about the continuation of the dipole-strength distribution below the threshold of the (γ, n) reaction.

The total photoabsorption cross section has been deduced by combining the present (γ, γ') data and the averaged (γ, n) data of Refs. [21,22]. In Fig. 17 this total cross section is compared with a Lorentz curve with the parameters given earlier. The extension of the GDR to energies below the particle threshold by a Lorentz curve was suggested in Ref. [39]. As can be seen in Fig. 17 the experimental cross section includes extra strength with respect to the approximation of the GDR by a Lorentz curve in the energy range from 6 to 11 MeV. According to the measurement with polarized photons described in Sec. II D we can assume $E1$ character for this extra strength, which amounts to about 2% of the Thomas-Reiche-Kuhn sum rule and may be related to a pygmy dipole resonance.

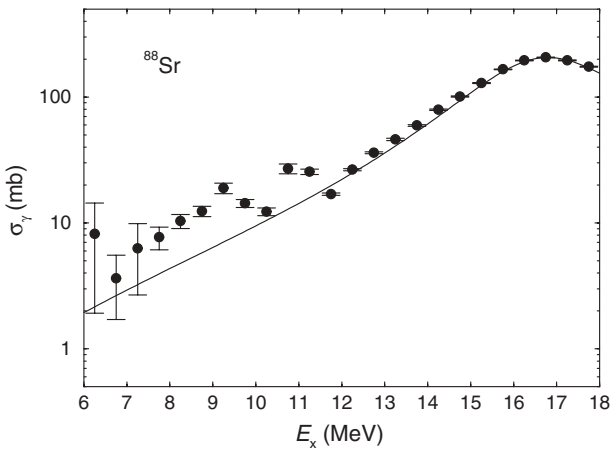

FIG. 17. Total photoabsorption cross section obtained by combining the present (γ, γ') data and the (γ, n) data of Refs. [21,22]. Starting from 6.0 MeV, the data were averaged over 0.5-MeV bins to reduce statistical fluctuations. For the (γ, n) data mean values of the data given in Refs. [21,22] have been used as those data disagree in the range between 11 and 13 MeV (cf. Fig. 16). The solid line shows a Lorentz distribution with the parameters given in Sec. III.

IV. SUMMARY

The dipole-strength distribution in ^{88}Sr up to the neutron-separation energy has been studied in photon-scattering experiments at the ELBE accelerator using various electron energies. Ground-state transitions have been identified by comparing the transitions observed at different electron energies. We identified 160 levels with a total dipole strength of about 200 meV/MeV^3. Spin $J = 1$ could be deduced from the angular correlations of the ground-state transitions for about 90 levels, including 84% of the total dipole strength. A measurement of linear polarizations of the γ rays by using polarized bremsstrahlung reveals that almost all transitions with energies greater than 6 MeV are $E1$ transitions. These $E1$ transitions comprise about 63% of the total dipole strength of all ground-state transitions.

The intensity distribution obtained from the measured spectra after a correction for detector response and a subtraction of atomic background in the target contains a continuum part in addition to the resolved peaks. It turns out that the dipole strength in the resolved peaks amounts to about 43% of the total dipole strength whereas the continuum contains about 57%.

An assignment of inelastic transitions to particular levels and, thus, the determination of branching ratios was possible only for a small number of levels. To get information about the intensities of inelastic transitions to low-lying levels we have applied statistical methods. By means of simulations of γ-ray cascades, intensities of branching transitions could be estimated and subtracted from the experimental intensity distribution and the intensities of ground-state transitions could be corrected on average for their branching ratios.

A comparison of the photoabsorption cross section obtained in this way from the present (γ, γ') experiments with (γ, n) data shows a smooth connection of the data of the two different experiments and gives new information about the extension of the dipole-strength distribution toward energies around and below the threshold of the (γ, n) reaction. In comparison with a straightforward approximation of the GDR by a Lorentz curve one observes extra $E1$ strength in the energy range from 6 to 11 MeV, which is mainly concentrated in strong peaks for which multipolarity $E1$ was proven in the present experiments. This extra $E1$ strength may be considered as an indication of a pygmy dipole resonance.

ACKNOWLEDGMENTS

We thank the staff of the ELBE accelerator for their cooperation during the experiments and acknowledge the technical assistance of A. Hartmann and W. Schulze. We are especially grateful to F. Bečvář, M. Krtička, F. Dönau, and S. Frauendorf for useful discussions. We thank the Nuclear Physics Group at the University of Cologne for lending us the ^{88}Sr target. This work was supported by the Deutsche Forschungsgemeinschaft under Contract No. DO466/1-2.

[1] M. Arnould and S. Goriely, Phys. Rep. **384**, 1 (2003).
[2] G. A. Bartholomew, E. D. Earle, A. J. Ferguson, J. W. Knowles, and M. A. Lone, Adv. Nucl. Phys. **7**, 229 (1973).
[3] S. Goriely, Phys. Lett. **B436**, 10 (1998).
[4] A. Zilges, M. Babilon, T. Hartmann, D. Savran, and S. Volz, Prog. Part. Nucl. Phys. **55**, 408 (2005).
[5] S. Goriely and E. Khan, Nucl. Phys. **A706**, 217 (2002).
[6] S. Goriely, E. Khan, and M. Samyn, Nucl. Phys. **A739**, 331 (2004).
[7] P. Axel, K. K. Min, and D. C. Sutton, Phys. Rev. C **2**, 689 (1970).
[8] S. Datta and J. S. Allen, Phys. Rev. C **8**, 1421 (1973).
[9] R. M. Laszewski, R. Alarcon, and S. D. Hoblit, Phys. Rev. Lett. **59**, 431 (1987).
[10] R. Alarcon, R. M. Laszewski, A. M. Nathan, and S. D. Hoblit, Phys. Rev. C **36**, 954 (1987).
[11] U. Kneissl, N. Pietralla, and A. Zilges, J. Phys. G **32**, R217 (2006).
[12] R. Schwengner, R. Beyer, F. Dönau, E. Grosse, A. Hartmann, A. R. Junghans, S. Mallion, G. Rusev, K. D. Schilling, W. Schulze, and A. Wagner, Nucl. Instrum. Methods A **555**, 211 (2005).
[13] F. R. Metzger, Phys. Rev. C **15**, 2253 (1977).
[14] F. R. Metzger, Nucl. Phys. **A173**, 141 (1971).
[15] F. R. Metzger, Phys. Rev. C **11**, 2085 (1975).
[16] G. Isoyama, T. Ishimatsu, E. Tanaka, K. Kageyama, and N. Kumagai, Nucl. Phys. **A342**, 124 (1980).
[17] K. Wienhard, C. Bläsing, K. Ackermann, K. Bangert, U. E. P. Berg, K. Kobras, W. Naatz, D. Rück, R. K. M. Schneider, and R. Stock, Z. Phys. A **302**, 185 (1981).
[18] N. Pietralla, V. N. Litvinenko, S. Hartman, F. F. Mikhailov, I. V. Pinayev, G. Swift, M. W. Ahmed, J. H. Kelley, S. O. Nelson, R. Prior, K. Sabourov, A. P. Tonchev, and H. R. Weller, Phys. Rev. C **65**, 047305 (2002).
[19] L. Käubler, H. Schnare, R. Schwengner, H. Prade, F. Dönau, P. von Brentano, J. Eberth, J. Enders, A. Fitzler, C. Fransen, M. Grinberg, R.-D. Herzberg, H. Kaiser, P. von Neumann-Cosel, N. Pietralla, A. Richter, G. Rusev, Ch. Stoyanov, and I. Wiedenhöver, Phys. Rev. C **70**, 064307 (2004).
[20] A. J. Koning, S. Hilaire, and M. C. Duijvestijn, AIP Conf. Proc. **769**, 1154 (2005).
[21] A. Lepretre, H. Beil, R. Bergere, P. Carlos, A. Veyssiere, and M. Sugawara, Nucl. Phys. **A175**, 609 (1971).
[22] A. M. Goryachev and G. N. Zalesnyy, Vopr. Teor. Yad. Fiz. **8**, 121 (1982).
[23] F. Ajzenberg-Selove and J. H. Kelley, Nucl. Phys. **A506**, 1 (1990).
[24] CERN Program Library Long Writeup W5013, Geneva, 1993 (unpublished).
[25] E. Haug (private communication).
[26] G. Roche, C. Ducos, and J. Proriol, Phys. Rev. A **5**, 2403 (1972).
[27] F. Salvat, J. D. Martinez, R. Mayol, and J. Parellada, Phys. Rev. A **36**, 467 (1987).
[28] M. May and G. C. Wick, Phys. Rev. **81**, 628 (1951).
[29] C. E. Porter and R. G. Thomas, Phys. Rev. **104**, 483 (1956).
[30] G. Rusev, Ph.D. dissertation, Technische Universität Dresden, 2007 (unpublished).
[31] F. Bečvář, Nucl. Instrum. Methods A **417**, 434 (1998).
[32] T. von Egidy and D. Bucurescu, Phys. Rev. C **72**, 044311 (2005).

[33] T. A. Brody, J. Flores, J. B. French, P. A. Mello, A. Pandey, and S. S. M. Wong, Rev. Mod. Phys. **53**, 385 (1981).
[34] Y. Kalmykov, T. Adachi, G. P. A. Berg, H. Fujita, K. Fujita, Y. Fujita, K. Hatanaka, J. Kamiya, K. Nakanishi, P. von Neumann-Cosel, V. Yu. Ponomarev, A. Richter, N. Sakamoto, Y. Sakemi, A. Shevchenko, Y. Shimbara, Y. Shimizu, F. D. Smit, T. Wakasa, J. Wambach, and M. Yosoi, Phys. Rev. Lett. **96**, 012502 (2006).
[35] P. Axel, Phys. Rev. **126**, 671 (1962).
[36] P. Ring and P. Schuck, in *The Nuclear Many Body Problem* (Springer, New York, 1980).
[37] http://www-nds.iaea.org/RIPL-2/.
[38] T. Rauscher and F.-K. Thielemann, At. Data Nucl. Data Tables **88**, 1 (2004).
[39] C. B. Dover, R. H. Lemmer, and F. J. W. Hahne, Ann. Phys. (NY) **70**, 458 (1972).